Atmos. Chem. Phys. Discuss., 13, 18809–18853, 2013
www.atmos-chem-phys-discuss.net/13/18809/2013/
doi:10.5194/acpd-13-18809-2013

Atmospheric Chemistry and Physics Discussions

A new method for evaluating the impact of vertical distribution on aerosol radiative forcing in general circulation models

M. R. Vuolo[1,*], M. Schulz[2,1], Y. Balkanski[1], and T. Takemura[3]

[1]Laboratoire des Sciences du Climat et de l'Environnement (LSCE), CEA-UVSQ-CNRS UMR 8212, Institut Pierre et Simon Laplace, L'Orme des Merisiers, F-91191 Gif sur Yvette Cedex, France
[2]Norwegian Meteorological Institute, Henrik Mohns Plass 1, 0313 Oslo, Norway
[3]Research Institute for Applied Mechanics, Kyushu University, 6-1 Kasuga-koen, Kasuga, Fukuoka 816-8580, Japan
[*]now at: Institut National de la Recherche Agronomique, UMR Environnement et Grandes Cultures, Route de la Ferme, 78850 Thiverval-Grignon, France

Received: 17 May 2013 – Accepted: 18 June 2013 – Published: 15 July 2013

Correspondence to: M. R. Vuolo (mrvuolo@gmail.com)

Published by Copernicus Publications on behalf of the European Geosciences Union.

Abstract

The quantification and understanding of direct aerosol forcing is essential in the study of climate. One of the main issues that makes its quantification difficult is the lack of a complete comprehension of the role of the aerosol and clouds vertical distribution. This work aims at reducing the incertitude of aerosol forcing due to the vertical superposition of several short-lived atmospheric components, in particular different aerosols species and clouds. We propose a method to quantify the contribution of different parts of the atmospheric column to the forcing, and to evaluate model differences by isolating the effect of radiative interactions only. Any microphysical or thermo-dynamical interactions between aerosols and clouds are deactivated in the model, to isolate the effects of radiative flux coupling. We investigate the contribution of aerosol above, below and in clouds, by using added diagnostics in the aerosol-climate model LMDz. We also compute the difference between the forcing of the ensemble of the aerosols and the sum of the forcings from individual species, in clear-sky. This difference is found to be moderate on global average (14 %) but can reach high values regionally (up to 100 %). The non-additivity of forcing already for clear-sky conditions shows, that in addition to represent well the amount of individual aerosol species, it is critical to capture the vertical distribution of all aerosols. Nonlinear effects are even more important when superposing aerosols and clouds. Four forcing computations are performed, one where the full aerosol 3-D distribution is used, and then three where aerosols are confined to regions above, inside and below clouds respectively. We find that the forcing of aerosols depends crucially on the presence of clouds and on their position relative to that of the aerosol, in particular for black carbon (BC). We observe a strong enhancement of the forcing of BC above clouds, attenuation for BC below clouds, and a moderate enhancement when BC is found within clouds. BC forcing efficiency amounts to 44, 171, 333 and 178 $\mathrm{W\,m^{-2}}$ per unit optical depth for BC below, within, above clouds and for the 3-D BC distribution, respectively. The different behaviour of forcing nonlinearities for these three components of the atmospheric column suggests that, an important reason for

ACPD
13, 18809–18853, 2013

differences between cloudy-sky aerosol forcings from different models may come from different aerosol and clouds vertical distributions. Our method allows to evaluate the contribution to model differences due to aerosol and clouds radiative interactions only, by reading 3-D aerosol and cloud fields from different GCMs, into the same model. This method avoids differences in calculating optical aerosol properties and forcing to enter into the discussion of inter-model differences. It appears that the above and in-cloud amount of BC is larger for SPRINTARS (190 compared to 179), increasing its cloudy-sky forcing efficiency with respect to LMDz, being thus potentially an important factor for inter-model differences.

1 Introduction

Quantifying the effect of the vertical overlapping of atmospheric components on the radiative fluxes is not a straightforward problem, as the forcing is non-linear with respect to the aerosol amount (Charlson et al., 1992). From a modeling point of view, it is necessary to deal with multiple scattering among layers (non-linear processes) and the strong dependency on the scattering and absorbing characteristics of the superposed layers (Meloni et al., 2005; Gómez-Amo et al., 2010). From an experimental point of view, the technology of active remote sensing, that allows for a vertically-resolved study of the atmospheric components, is relatively recent and does not provide information behind optically thick objects, e.g. below clouds viewed from space (Chepfer et al., 2008; Vuolo et al., 2009; Koffi et al., 2012). Concerning the coexistence of different aerosols within the same atmospheric column, many works have assumed that for externally mixed aerosols, the effects of individual aerosol species add linearly to constitute the total forcing (Podgorny et al., 2001; Boucher et al., 2001; Reddy et al., 2005). The effect of clouds below absorbing aerosols has been studied since the late 90s by means of column radiative models (Haywood et al., 1997; Liao et al., 1998; Zarzycki et al., 2010), general circulation models (e.g. Haywood et al., 1998) and more recently using satellite data (Chand et al., 2008; Peters et al., 2011), but the aerosol forcing in

ACPD
13, 18809–18853, 2013

all- and cloudy-sky remains highly uncertain (Schulz et al., 2006; Myhre et al., 2013). Some studies on radiative forcing use the assumption that aerosols effects are negligible in cloudy regions as they are "masked" by clouds. (e.g. Bellouin et al., 2008; Evan et al., 2009: Supporting Online Material).

A column model has the advantage that one may isolate a single physical effect; however, it requires many assumptions to demonstrate the importance of the effect for the real atmosphere. GCMs or CTMs are more suitable to estimate the impact of a phenomenon on the global scale. Haywood et al. (1998) studied the dependency of forcing on the vertical position of aerosols, and the effect of clouds, by concentrating all the aerosol content in only one model level, from surface to 25 km. They find that BC forcing for the same BC burden varies with increasing altitude from 0.45 $W m^{-2}$ to 0.9 $W m^{-2}$. More recently, black carbon direct forcing divided by the burden, computed as a function of altitude in a 3-D CTM, is reported to increase considerably with height (Samset and Myhre, 2011), ranging from 380 $W g^{-1}$ at 1000 hPa, up to 3800 $W g^{-1}$ at 20 hPa. The dependency of the BC radiative forcing from the vertical profile has been estimated to be responsible of 20 to 50 % of the spread in forcing values of AeroCom models, by use of a common forcing efficiency vertical profile (Samset et al., 2013). This sensitivity of forcing to vertical distribution is expected to be responsible for an important part of the actual inter-model forcing differences. A comparison of aerosol vertical distributions with respect to CALIOP observations (Koffi et al., 2012) shows a large spread in the distribution simulated by General Circulation Models.

This study aims to quantify in more detail the sensitivity of forcing to vertical position of aerosols, using realistic aerosol and cloud distributions, and focusing on the relative position of distinct aerosol and cloud layers. It documents the importance of the vertical superposition of aerosol (primarily black carbon) with clouds and the superposition of distinct aerosol layers, at the global scale. We analyse the role of the relative vertical position of several atmospheric agents by quantifying the nonlinearity of forcing, i.e., the difference between the actual forcing and the sum of the forcings of the individual components. This is done for different combinations of aerosol and cloud layers, realized

ACPD
13, 18809–18853, 2013

in our specific model set-up, where we identify aerosols above, below and in clouds in the cloudy area. These nonlinearities allow us to quantify: (1) the amount of the error when considering the total forcing as the sum of the forcings of the individual components, (2) the importance of a correct representation of the "vertical layering" (that is, which aerosol component is below and which one is above). We will show that, for the same aerosol optical thickness of an aerosol component, its position relative to that of other species and clouds has a large impact on the resulting forcing. As the cloudy- and all-sky forcing is highly variable among GCMs (Schulz et al., 2006; Myhre et al., 2013), we finally illustrate the impact of the vertical position of BC and clouds on this variability, by introducing in the same host model the 3-D fields of aerosols and clouds from two different models, and computing forcing differences. In this way, the spatial distribution of aerosols and clouds affect the forcing differences, while other factors like surface albedo, aerosol optical properties, meteorological and radiative computations, have no impact, because they are computed by the same host model.

2 Atmospheric TOA forcing due to the position of cloud and aerosol layers

The radiative forcing is the change in net radiative flux at the tropopause due to a perturbation introduced by an atmospheric agent (IPCC). Here, we consider only the shortwave contribution to the aerosol forcing, as the longwave forcing is a negligible part of the direct aerosol forcing except for dust and, to a smaller extent, for sea salt (Reddy et al., 2005). If interactions occur between the added atmospheric agent and the environment, the forcing will depend on the environment (for instance, a cloudy environment for aerosols). In the same way, if two atmospheric agents (for example aerosols and clouds or two distinct aerosol species) interact amongst themselves, the total forcing will be different from the sum of the forcings from the individual components.

Indeed, we can easily show that the two effects are physically equivalent, according to the definition of forcing. Call $F(A)$ the net TOA flux that incorporates the atmospheric agent "A" only, and RF(A) the radiative forcing from "A". Call dRF the difference between

ACPD
13, 18809–18853, 2013

the forcing of agent "A" in an environment where "B" is present (RF($A|B$)) minus the forcing of "A" alone (RF(A)):

$$\mathrm{dRF} = \mathrm{RF}(A|B) - \mathrm{RF}(A) = F(A+B) - F(B) - [F(A) - F(\mathrm{clear})], \quad (1)$$

where $F(A+B)$ is the flux computed with both agents "A" and "B". Now we add and subtract F(clear):

$$\begin{aligned}\mathrm{dRF} &= F(A+B) - F(\mathrm{clear}) - [F(B) + F(A) - 2F(\mathrm{clear})] \\ &= \mathrm{RF}(A+B) - \mathrm{RF}(A) - \mathrm{RF}(B).\end{aligned} \quad (2)$$

That is, the difference dRF coincides with the difference between the forcing of the ensemble of the agents minus the sum of the forcings of the individual components. See the Appendix and Fig. 1 for more details.

The interaction between atmospheric agents (aerosols and clouds) can be of several kinds. The potential of aerosols to modify clouds optical properties is referred to as the first indirect effect (e.g. Twomey, 1991). Aerosols can also modify cloud microphysics through the second indirect effect (e.g. Albrecht, 1989). Moreover, absorbing aerosols can alter the atmospheric temperature profile, which impacts convection and cloud formation (semi-direct effect, e.g. Hansen et al., 1997). Another kind of interaction is the one that occurs because of the exchange of radiation between two superposed layers of aerosols and clouds. In the framework of this study, only the last mentioned form of interaction is investigated. To achieve this objective, we eliminate semi-direct and indirect effects to better understand the effect of the exchanges of radiation between superposed layers (the Sect. 3.4.3 below explains how this is done in the framework of this study).

ACPD
13, 18809–18853, 2013

3 Method

3.1 LMDz host model and aerosol optical parameters

The model used in our experiments is the general circulation model LMDz (Hourdin et al., 2006), with 95 × 96 horizontal resolution and 19 vertical levels. Meteorology is nudged with ECMWF reanalysis winds (Simmons et al., 2006) and HADiSST sea surface temperatures (Rayner et al., 2003). Aerosol fields are read as input of the model from monthly averages, and in the reference experiment (see Sect. 2.4) these aerosols fields are the AeroCom median model results for 2006. The aerosol concentration at each time step is computed in LMDz by linear interpolation of the monthly mean values. The model accounts for the following four basic properties that influence optical parameters of the ambient aerosol: size, chemical composition, hygroscopicity and mixing state of the particles.

The size of the aerosol is represented in LMDz through a superposition of lognormal distributions. In this work, we treat the sulphate, BC and organic carbon (OC) as external mixtures. Submicron aerosols are transported into two distinct modes, one that is soluble (rather hygroscopic) and a second one that is insoluble. We keep track of both soluble and insoluble BC and POM. We assume that primary, insoluble carbonaceous particles become soluble with time. The half life of ageing for BC and POM is taken as 1.1 days based upon Cooke and Wilson (1996). A ratio POM : OC = 1.4 : 1 was used. This value corresponds to the low range of the values reported in Turpin et al. (1999).

The uptake and loss of water on aerosol particles (hygroscopicity) is generally fast and depends on the chemical composition, size and surface properties of the aerosol particle. Hygroscopic growth (HG) of aerosol particles is a major factor that determines the optical parameters of an aerosol population. The model takes into account the observation that two particles with different HG factors appear upon hydration of dry particles of a given diameter. This separation is represented through the two modes: a soluble one and an insoluble one. HG changes the particle diameter, the aerosol composition and particle surface characteristics. It is computed as a function of chem-

ACPD
13, 18809–18853, 2013

ical composition in each mode. The parameterization follows initial ideas of Gerber's experimental work (Gerber, 1988). Gerber had established an approximate formula for aerosol growth behaviour of rural aerosol and sea salt. Our first assumption is that the hygroscopic growth of the ambient aerosol lies in between that of sea salt and of rural aerosol and is a linear function of the aerosol composition. In the case of an externally mixed aerosol, BC, OC and SO_4 are then considered separately to determine their optical properties. The wet diameter of the aerosol is used to determine the optical properties of the individual components from a look-up table which accounts for the ambient relative humidity in the model gridbox. The overall optical properties of the global aerosol are then computed by summing the different contributions of the aerosol components to the extinction. For the single scattering albedo, the different contributions are weighted with the respective specific extinction coefficients, and for the asymmetry parameter by the product of the specific extinction and the single scattering albedo.

3.2 Radiative computations in LMDz

The shortwave radiative fluxes in the model LMDz are computed with the scheme developed in (Fouquart et al., 1980), both for clear- and cloudy-sky; the shortwave spectrum is divided into two spectral intervals: 0.25–0.68 µm and 0.68–4.00 µm. The reflectivity and transmissivity of a grid cell are computed using the random cloud overlap assumption (Morcrette et al., 1986) by weighting linearly the clear and cloudy sky fluxes with their respective fractions in the cell. The aerosols direct and indirect effects have been introduced by (Quaas et al., 2004), following (Boucher et al., 2002). In the default LMDz parametrization of the radiative effects of aerosols and clouds, direct and indirect effects (when activated) are taken into account in both forcing and meteorological fields computations. Indeed, forcing is computed as the difference between the flux that incorporates aerosols effects minus a flux computed without aerosol contribution, both in clear and cloudy sky conditions. The fluxes that incorporate aerosol and clouds effects are also used to impose the radiative-convective equilibrium of the at-

ACPD
13, 18809–18853, 2013

mospheric column. This explains why different aerosol and cloud fields in LMDz give rise, by default, to different meteorological fields.

3.3 Diagnosis of forcings and forcing efficiencies

In this study, we use as reference a completely aerosol-free atmosphere as was done in previous studies (Satheesh et al., 1999; Podgorny et al., 2001; Takemura et al., 2002; Reddy et al., 2005). This reference assures that there will be no dependency on the definition, spatial distribution and optical properties of pre-industrial aerosols, as this also is subject to uncertainties and can be different from one model to another (Visser et al., 2000). Thus, the direct radiative forcings are computed as the difference between the net TOA flux with and without aerosols, both in clear and cloudy sky conditions (RF_{CS}, RF_{CL}), for each species separately (BC, SO_4, POM, DUST, SS) and for the ensemble of all the species "AER". All-sky radiative forcing, RF_{AS}, is calculated at each time step, and for each model cell, as:

$$RF_{AS} = (1 - CLT) \cdot RF_{CS} + CLT \cdot RF_{CL}, \quad (3)$$

where CLT is the cloudy fraction in each grid cell. We compute clear- and cloudy-sky forcing efficiencies and relate them to the vertical positions (see below). The characteristic height of aerosols and clouds is computed by weighting their vertical coordinate with their optical thickness. The clear-sky forcing efficiency per unit aerosol optical depth NRF_{CS} is computed as RF_{CS}/AOD, with RF_{CS} and AOD being yearly average values of clear-sky forcing and optical depth. Analogously, the cloudy-sky forcing efficiency is computed as the ratio of the global averages of RF_{CL} and AOD. We avoid computing efficiency with instantaneous 2-D fields of forcing and optical depth because it requires the choice of a threshold for the optical depth to avoid numerically occuring, but unrealistic high values of efficiency when AOD is very low. Also – such a choice can not be the same for each aerosol species, which would require different threshold values of optical depth.

ACPD
13, 18809–18853, 2013

3.4 Model simulations

We developed a method that we propose here to study the dependency of forcing on the vertical distribution of aerosols and clouds. Two questions are addressed: what is the contribution to the forcing from aerosols below, inside and above clouds, and, what is the potential difference between two models results introduced by different aerosols and clouds vertical distributions? The method requires multiple model runs where the radiative forcing due to specific fractions of the aerosol burden is computed. These runs are classified below in terms of model "configurations" and "experiments". Aerosol and cloud fields are read from previously realized atmospheric chemistry simulations, performed with the host model LMDz and with the model SPRINTARS (Takemura et al., 2005). Other host model factors like resolution, solar fluxes, surface albedo, intensive aerosol optical properties etc., are invariable between the runs.

To quantify the amount of inter-model forcings differences that can be attributed to different aerosols and clouds vertical distributions, we run the model LMDz in 5 different "configurations", while to attribute the forcing to aerosols below, inside and above clouds we perform, for each "configuration", 4 different "experiments".

3.4.1 The "configurations"

The five configurations differ in the origin of the aerosol and eventually cloud fields that are read into the model LMDz. They are defined as follows:

1. The "default" configuration: monthly fields of aerosols from a previous model run are read as input, and cloud fields are computed interactively at each time step.
2. The "reading LMDz" configuration: the same monthly aerosols as in configuration "1" are read, but daily cloud fields from the default configuration are also read and are used in the radiation code.
3. The "reading SPRINTARS" configuration: as configuration "2", but monthly aerosol fields and daily cloud fields come from the model SPRINTARS.

ACPD
13, 18809–18853, 2013

4. The “reading LMDz aerosols – SPRINTARS clouds” configuration: monthly aerosol fields are read from LMDz and daily cloud fields come from SPRINTARS.

5. The “reading SPRINTARS aerosols – LMDz clouds” configuration: monthly aerosol fields are read from SPRINTARS and daily cloud fields come from LMDz

We use configuration “2” and not “1” for comparisons with the other configurations, because often only daily-averaged fields are accessible from another model, such as SPRINTARS. The time step of 30 min in our LMDz model produces a higher variability in cloud fields, which introduces differences to a configuration reading in daily cloud fields. Similarly, to avoid differences coming from the different spatial resolution of the cloud fields read as input from the SPRINTARS model, these fields were regridded onto the LMDz resolution.

3.4.2 The “experiments”

With the “default configuration”, we first perform a simulation with the full 3-D aerosol distribution produced by default by the model. This baseline run will be referred to as the “reference simulation”. Then, for each of the 5 abovementioned configurations, we perform the 4 following “experiments”:

1. Experiment “aib” (above-inside-below), with the full 3-D aerosol distribution produced by default by the model, and no aerosol in completely clear columns.

2. Experiment “abv” (above), with aerosols only above the highest cloudy model layer.

3. Experiment “in” (inside), with aerosols only between the lowest and the highest cloudy layers.

4. Experiment “blw” (below), with aerosols only below the lowest cloudy level.

We determine cloud lowest and highest levels at each model time step, using cloud fraction and cloud extinction thresholds together. A no-cloud state is defined for the

ACPD
13, 18809–18853, 2013

grid cell where cloud fraction is below a threshold of 0.001 or cloud extinction is below a threshold of 0.01 km^{-1}, a value that is 3 orders of magnitude smaller than the typical observed cloud extinction coefficients (Li et al., 2011). Starting from the lowest model layer, we check if the cloud fraction and extinction are larger than the corresponding thresholds. If the condition is fulfilled for at least one level, the column is considered (partially) cloudy, and the first level that fulfills the condition is taken as the cloud bottom. Then, the same check is effectuated for the same column, starting from model uppermost level, to find cloud top. Multi-layer clouds are not identified with this method, and the experiment "in" incorporates both aerosols inside a cloud and embedded in multi-layer clouds. In the experiments "aib", "abv", "in" and "blw", we put to zero aerosol optical depths if the column is completely clear, so that the distributions "abv", "in" and "blw" of aerosol optical depth sum up to the "aib" one. The difference in total optical depth brought about by this correction with respect to the "reference simulation" (full 3-D aerosol distribution) will be discussed below in Sect. 4.

The combination of the 5 "configurations" and the 4 "experiments", plus the "reference simulation" of the proposed method constitutes an ensemble of 21 runs.

3.4.3 New options implemented in the LMDz radiative module

In a General Circulation Model (GCM) the feedbacks of aerosols and clouds on meteorological fields (see Sect. 3.2) prevent us to clearly interpret the forcing differences among runs. Simulations with different aerosols spatial distributions wouldn't be comparable if feedbacks on cloud, wind, temperature and relative humidity fields took place. Furthermore, we want to isolate here the effect of cloud layers on the direct aerosol radiative forcing without having additional microphysical and dynamical interactions (indirect and semi-direct effects). To achieve these objectives, we have implemented in LMDz the options to:

1. switch off the feedbacks from aerosols on the meteorology
2. read in as input cloud fields

ACPD
13, 18809–18853, 2013

3. use two different cloud fields, one for the diagnostics of radiative forcing and the other for the meteorology (by default, the model works with only one cloud field).

To deactivate the aerosol feedback on meteorology (point 1), we call twice the radiation computations: once with the aerosols fields (to diagnose forcings) and once without any aerosol (to compute the feedback of radiative fluxes on meteorology). This means that we neglect aerosols feedback on climate (through indirect and semi-direct effect).

To compute forcing with arbitrary cloud fields (point 2), we added a routine in the model that reads daily fields of cloud optical depths and of cloud fractions.

Concerning clouds feedbacks on meteorology (point 3), we cannot simply "switch them off" as we do for aerosols. Cloud impacts on the thermodynamical balance of the atmosphere are important and we have to take them into account to have realistic temperature and humidity fields. Nevertheless, we don't wish to get a different cloud feedback for each configuration we use. In the three configurations "default", "reading LMDz" and "reading SPRINTARS", three different cloud fields are used for fluxes computations: the "on-line" cloud field produced by default by the model, the daily averaged field in output from configuration (1), and the SPRINTARS daily-averaged field, respectively.

To avoid three different feedbacks on meteorology, we introduced in the radiative code a double computation of cloudy-sky fluxes, one used for meteorology, the other used for forcing computations:

1. The first is the cloudy-sky flux computation with the clouds produced interactively by the model. These clouds are the same for all the configurations/experiments, as the host model LMDz remains unchanged. Moreover, the difference in aerosol fields in the configurations/experiments has no impact on the cloud field, as we previously deactivated any aerosol feedback. We use these fluxes, which include the effect of the "interactively computed clouds", as input for meteorology computations.

ACPD
13, 18809–18853, 2013

2. The second computation of the cloudy-sky fluxes is the one that takes into account the cloud fields that are read in, and these change according to the "configuration". We use these fluxes to diagnose forcings.

With the implementation of these new options in the host model, all the meteorological fields are identical in the 21 runs we perform, but we can still diagnose different forcings due to different clouds and aerosols fields. We checked that "interactively computed" cloud fields, as well as temperature and humidity fields, are exactly the same for all our runs (not shown).

4 Results

4.1 Clear-sky and cloudy sky forcing in reference simulation

In this section we discuss the forcing and forcing efficiencies obtained for the full model run in the "default configuration", our "reference simulation". Table 1 shows the average values of optical depth, burden and clear-, cloudy- and all-sky forcings, while Fig. 2 shows the spatial distribution of these latter forcings, and of the cloud fraction. Note again that, for simplicity and to limit the numbers of experiments, we have defined and computed forcing here as the sum of anthropogenic and natural direct aerosol radiative effects, measured against a zero aerosol background in the radiative computations.

The total aerosol forcing using the total aerosol optical properties ("AER") is $-2.39\,\mathrm{W\,m^{-2}}$ in clear-sky conditions and $-1.19\,\mathrm{W\,m^{-2}}$ in all-sky conditions. All the species exhibit negative top-of-the-atmosphere forcing except for BC. Total sulfate all-sky forcing is $-0.47\,\mathrm{W\,m^{-2}}$, and is in the range of the anthropogenic forcing values recently found by Myhre et al. (2013) (-0.11 to $-0.48\,\mathrm{W\,m^{-2}}$), in particular when accounting for a 20 % natural contribution. The total BC forcing of $+0.38\,\mathrm{W\,m^{-2}}$ is considerably lower than the total BC estimated by Bond et al. (2013) ($+0.88\,\mathrm{W\,m^{-2}}$), mainly due to differences in emissions (with lower emissions assumed in this work). This forcing corresponds to the range of anthropogenic fossil fuel and biofuel BC forcing re-

ACPD
13, 18809–18853, 2013

ported by Myhre et al., 2013 (+0.05 to +0.37 $W m^{-2}$) where similar emissions where assumed. The cloud fraction given in Table 1 ($CLT^{\#}$) corresponds to the mean of the monthly cloud fraction field, weighted by the clear-sky forcing field. Figure 2 indicates higher cloud fractions in the marine regions with high sea salt burden (hence sea salt clear-sky forcing), than in desert regions with higher dust burden.

Table 1 also reveals the importance of the cloudy-sky forcing (RF_{CL}) in particular for BC, reflected by its magnitude and forcing efficiency. Cloudy-sky forcings are quite different from the corresponding clear-sky values for all species. If the clouds had no effect on the aerosols forcing, the clear-sky and cloudy-sky aerosol forcings would be the same. Note that the cloudy sky forcings reported in Table 1 are always more positive (or less negative) than the corresponding clear-sky forcings. POM cloudy-sky forcing even changes sign with respect to the clear-sky value.

Table 1 shows the all-sky forcing estimated with a simple "cloud mask" hypothesis (e.g. Bellouin et al., 2008; Evan et al., 2009). Here we use annual fields of clear-sky forcing and cloud fraction: $RF_{AS}{}^{*} = (1 - CLT^{\#})RF_{CS}$. The simple cloud-mask approximation gives all-sky forcing values that differ significantly from the "true" ones. In particular a much too low value of BC positive forcing is observed, showing that half of the black carbon forcing can be attributed to other than masking effects in cloudy regions.

4.2 Forcing contributions from below, above and within clouds

Where in the vertical column of the cloudy sky is the redistribution of radiative energy located? Further insight comes from the results of the experiments "aib", "abv", "in", "blw" using the "default configuration". Table 2 gives the values of AOD^{*}, forcings and forcing efficiencies for these experiments. The cloud level information in each column at any given moment is used to obtain global averages. Note again, that we have excluded the grid columns where no clouds are present from the averages (see Sect. 3). Excluding these columns has a small impact on the results. Aerosol optical depths in the full-scale reference simulation are compared in Table 1 to the "cloud-containing-column"

ACPD
13, 18809–18853, 2013

AOD*, obtained in the "aib" experiment. They are only about 10 % higher, except for dust, where the difference is found to be 31 %. This is due to high dust loads appearing in very dry regions, where even our coarse GCM simulates no clouds and where thus the corresponding AOD is excluded from being taken into account for a global average AOD*.

The example of BC allows to appreciate the effect of vertical position of aerosol on clear-sky forcing efficiency. BC forcing efficiency (NRF_{CS}) equals on average 118 $W m^{-2}$ per unit optical depth in the "aib" experiment (Table 2). It varies from 82 to 126 $W m^{-2}$ when passing from the experiment "blw" to "abv". In the BC_{ABV} experiment, absorption of shortwave radiation is therefore 54 % stronger than in the BC_{BLW} experiment. One reason is, that at higher altitudes atmospheric molecules intercept less of the incoming radiation before it can interact with BC. This model behaviour is in agreement with Haywood and Ramaswamy (1998) and Samset and Myhre (2011), but we quantify here the effect for three distinct portions of the column. For comparison with cloudy sky, it is interesting to notice from Table 2 that cloudy-sky forcing efficiency (NRF_{CL}) is 178 $W m^{-2}$ per unit optical depth in the "aib" experiment, and varies from 44 to 333 $W m^{-2}$ when passing from below to above clouds. That is, BC_{ABV} is 650 % more efficient than the BC_{BLW} in absorbing incoming shortwave radiation when clouds are present.

We inspect further the cloudy sky forcing and forcing efficiency and compare them to the clear sky counterparts. The relative difference $(RF_{CL} - RF_{CS})/|RF_{CS}|$ in Table 2 quantifies the enhancement (if it has the same sign as RF_{CS}) or attenuation (if opposite sign) of the aerosol forcing due to the presence of clouds. This relative difference has the advantage of being weakly sensitive to aerosol horizontal distribution, as cloudy- and clear-sky forcings are similarly influenced by surface albedo.

As for the reference simulation (see Sect. 4.1), for the "aib", "abv" and "in" experiments the relative differences $(RF_{CL} - RF_{CS})/|RF_{CS}|$ are positive for all aerosol species (see Table 2). This means that all aerosol forcings are attenuated except for BC, since the clear-sky forcing is positive for BC and negative for all the other species. Except

ACPD
13, 18809–18853, 2013

for sulphate, these relative differences in the "abv" experiment are much more important than in "aib". For black carbon for example, the forcing enhancement by clouds is 52 % for the "aib" and 163 % for the "abv" experiments respectively. This signifies that the region above the clouds dominates the cloudy-sky forcing. In the "abv" experiment, POM, DUST and SS even change sign (become positive) when passing from clear to cloudy sky. This positive cloudy-sky forcing reflects that, even if the considered species is not absorbing at all (such as sea salt), more incoming shortwave radiation is trapped in between the aerosol and the cloud layer by the slightly absorbing air molecules. In the "blw" experiment, all differences $RF_{CL} - RF_{CS}$ are positive except for BC, meaning that below clouds all forcings are attenuated. Interestingly the cloudy-sky aerosol forcing below clouds does not become zero, indicating that thin clouds and cloud overlap assumptions in the model allow for an aerosol effect even when present below the lowest cloud layer. For black carbon, the forcing below clouds is attenuated by 47 % with respect to its clear-sky counterpart (Table 2, $(RF_{CL} - RF_{CS})/|RF_{CS}|$ for "blw" experiment). For the experiment "in" (BC between the lowest and the highest cloudy levels) the two effects of forcing attenuation and enhancement coexist, but the second one is prevailing. The relative difference $(RF_{CL} - RF_{CS})/|RF_{CS}|$ is indeed 64 % for BC in the "in" experiment, and the cloudy-sky forcing efficiency increases from 44 to 171 $W m^{-2} \tau^{-1}$ when passing from "blw" to "in" experiments (see Table 2, NRF_{CL} rows). This enhancing effect for BC within clouds may depend on the specific configuration of the clouds, for example low clouds of high albedo superposed by high optically thin clouds, and BC between them. Zarzycki et al. (2010) have shown that the cloud type is an important factor in the enhancement of BC forcing.

The three experiments seen together clearly show that the cloudy sky forcing efficiencies are much more sensitive to the vertical position of the aerosol than their clear-sky counterpart. Cloudy sky BC forcing efficiency "abv" versus "blw" is different by a factor of 8, while clear sky forcing "abv" versus "blw" is only enhanced by a factor 1.5.

ACPD
13, 18809–18853, 2013

4.3 BC forcing sensitivity to variable black carbon and cloud fields

This section is dedicated to the application of our method to the interpretation of inter-model spread in black carbon forcing estimates. We compare four possible different "configurations" and compute from monthly aerosol and daily cloud fields the black carbon radiative forcing. For this we use LMDz and SPRINTARS model output as described above and found as section-headers in Table 3. The different "experiments" "aib", "in", "blw" and "abv" have been done for all four "configurations". Only results for black carbon are analysed because it gives the largest contribution to cloudy-sky aerosol forcing and shows the largest variation of forcing and forcing efficiency passing from clear to cloudy sky and from below to above clouds.

The configuration "reading LMDz" and the configuration used in Sect. 4.2 differ in that daily mean cloud fields from the LMDZ reference simulation are used here, rather than the instantaneous model cloud fields (see Sect. 3.4.1). There are more areas partially cloudy in daily mean fields. As a result small differences appear for all parameters (compare Table 2, BC column with Table 3 upper part). The differences in cloudy-sky BC forcing are of the order of 5 % and less than 1 % in clear-sky conditions.

Such small differences even exist for global mean AOD, which is derived excluding totally cloud-free columns by setting AOD there to zero. As clouds fields for the "default" and "reading LMDz" configurations are respectively instantaneous and daily-averaged, aerosols optical depths are not exactly identical. The difference in optical depths between "default" and "reading LMDz" configurations amounts to about 4 %. This difference is small enough to consider the "reading LMDz" configuration representative of the "default" one, with the advantage of being unequivocally comparable to the "reading SPRINTARS" one. For SPRINTARS only daily mean clouds fields were available.

A direct comparison of the two model inputs can be found in Table 3 as global averages of forcings and forcing efficiencies for the "reading LMDz" and "reading SPRINTARS" configurations. We will denote as "relative difference": (SPRINTARS value –

ACPD
13, 18809–18853, 2013

LMDz value)/LMDz value. With this notation, in the case of the "aib" experiment the two models differ by −5 % for BC optical depth, by −3 % in clear-sky forcing, by −0.6 % in cloudy-sky forcing and by −6 % in all-sky forcing. Regionally the differences are much larger and can exceed 100 % (Fig. 5). Figure 4 represents the BC optical depths from "reading LMDz" and the differences to "reading SPRINTARS", for the experiments "aib", "abv", "in", "blw". Black carbon in SPRINTARS is less present at ground level, in continental regions, and has a higher fraction of total AOD_{BC} in the in-cloud region, except in a region in the Atlantic Ocean off Angola, where important negative differences of AOD_{BC} (SPRINTARS value – LMDz value) are observed. AOD_{BC} differences are in general positive for the experiment "abv", meaning that for SPRINTARS more BC is present above clouds. On global average, the vertical profiles of BC and clouds are given in Fig. 6 for "reading LMDz" and "reading SPRINTARS" configurations, and "aib", "abv", "in" and "blw" experiments.

Figure 5 shows the corresponding horizontal distribution patterns of clear-, cloudy- and all-sky forcings. Figure 5 illustrates that the regional differences between the two configurations can be very large, with larger differences for cloudy- than for clear-sky. This is not reflected by the above-mentioned global averaged differences. The differences in clear-sky forcings (Fig. 5, top right) reflect closely the differences in BC optical depth (Fig. 4, top right): SPRINTARS clear-sky forcing and optical depth is larger in East Asia and Indonesia and weaker in Africa and South America. All-sky forcing differences (Fig. 5, bottom-right) are quite similar to the clear-sky ones, with larger positive differences. As regards cloudy-sky forcings, the highest positive values of the difference are found over the coast of West Africa, in East Asia and Indonesia, and over the seas they are more important than their clear-sky counterparts. The split of BC optical depth in the "abv", "in" and "blw" experiment (Fig. 4) helps to understand this behaviour: SPRINTARS exceeds the LMDz cloudy-sky forcing in regions where also BC optical depth above and within clouds are higher in SPRINTARS, like over East Asia and over the Atlantic ocean far from the Angola coastline. Near this coastline, SPRINTARS shows significantly lower BC fraction within clouds (Fig. 4, "in" row), what

ACPD
13, 18809–18853, 2013

is producing the negative differences in cloudy-sky forcings observed in Fig. 5 (second line right). This is in agreement with the prevailing enhancement effect when BC is found within clouds, as discussed in the previous section.

In general, regions with negligible clear-sky forcing differences and important cloudy-sky forcing differences are related to a BC vertical distribution with the same load but a different vertical pattern. For SPRINTARS, a large part of the BC load is situated above the cloud top (see the positive values in Fig. 4, second line right).

In the "reading LMDz" and "reading SPRINTARS" configurations BC optical depth above clouds represents 29 %, and 32 % respectively, of the total and its contribution to the total cloudy sky BC forcing amounts in both cases to 54 % (Table 3). This reflects a significant nonlinearity between forcing and optical depth as a function of vertical position of BC with respect to clouds. For comparison, in clear-sky, the BC of the "abv" experiment contributes to the clear-sky forcing by 33 % for LMDz and by 31 % for SPRINTARS. Overall the efficiency NRF_{CL} for the "aib" experiment is larger for SPRINTARS than for LMDz (190 against 179, see Table 3). The larger fraction of BC optical depth above but also within clouds for SPRINTARS is responsible of this difference. Altogether it appears that even if the two all-sky forcings are not so different, the contributions from different regions and height levels are composed in a complex manner.

We also have performed the two "crossed simulations" corresponding to the configurations "reading LMDz aerosols – SPRINTARS clouds" and "reading SPRINTARS aerosols – LMDz clouds" (results are also shown in Table 3). Comparisons are this way possible for example for two configurations of e.g. reading LMDz aerosols. The changes in AOD values for corresponding experiments indicate that the clouds determine where aerosol is counted in our diagnostics, which excludes completely cloud-free columns. The overall BC cloudy sky forcing efficiency is the highest for the "reading SPRINTARS" and "reading LMDZ aerosols – SPRINTARS clouds" configuration, with values of 190 and 227 $W m^{-2}$ per unit optical depth (Table 3, "aib" column). This be-

ACPD
13, 18809–18853, 2013

haviour seems to be related to the vertical distribution of BC and clouds rather than to clouds characteristics.

Indeed, SPRINTARS clouds are optically thicker (see Table 4), so they have larger albedo (Twomey, 1974). If the clouds albedo were the main responsible of the model differences, BC aerosols above SPRINTARS clouds (optically thicker) would always have larger forcing efficiency than above LMDz clouds (optically thinner). Nevertheless, the two highest cloudy-sky normalized radiative efficiencies appear for LMDz aerosols above SPRINTARS clouds (333,W m^{-2}) and above LMDz clouds (328 W m^{-2}, see Table 3, "abv" column).

On the other hand, the overall NRF_{CL} for the different configuration has the same behaviour as the fraction of BC above and within clouds. The two configurations "reading SPRINTARS" and "reading LMDZ aerosols – SPRINTARS clouds", for which the NRF_{CL} is the highest, are also the ones that have the largest fraction of BC above and within clouds: 85 % and 88 % respectively, against 66 % and 69 % for the two other configurations.

We conclude that, for the range of clouds optical depths considered here, the enhancement of BC forcing by clouds, is primarily not sensitive to cloud characteristics but much more to the fraction of BC above and within clouds. Note again that the BC optical properties are the same for both models, since we are reading concentrations and compute optical properties during model run.

5 Discussion

5.1 Role of clouds and aerosol vertical positions for black carbon forcing

The effects of clouds and BC relative positions on BC forcing can be physically understood in the following way: when absorbing aerosols as BC are above clouds, underlying clouds are more reflective than the underlying surface, so that their presence amplifies the positive forcing. For scattering aerosols, the fact that clouds are more

ACPD
13, 18809–18853, 2013

reflective than the underlying surface determines a reduction of their negative forcing with respect to the clear-sky value. When aerosols are below clouds, the effect that prevails is the "cloud mask": aerosols intercept less incoming radiation, this reducing the magnitude of the forcing, regardless of sign.

We showed with the results of Sect. 4 how clouds enhance or attenuate BC forcing when BC is found above or below them, respectively. To explore regionally this role of clouds vertical position for BC forcing, now we look at the increment in BC forcing when passing from clear- to cloudy-sky, $dRF = RF_{CL}(BC) - RF_{CS}(BC)$. We report in Fig. 7 the horizontal distribution of yearly averaged dRF and of also the relative altitude of BC with respect to clouds, computed for each month j as:

$$(H(\mathrm{BC}) - H(\mathrm{CL}))_j = \left[\frac{\sum_i \mathrm{AOD}_{\mathrm{BC}}(z_i)\cdot(z_i)}{\sum_i \mathrm{AOD}_{\mathrm{BC}}(z_i)} - \frac{\sum_i \mathrm{COD}(z_i)\cdot(z_i)}{\sum_i \mathrm{COD}(z_i)}\right]_j \cdot (\mathrm{AOD}_{\mathrm{BC}}\cdot \mathrm{CLT})_j,$$

COD being the cloud optical depth, and z_i the height from the ground to the i-th model level. We multiply by the monthly values of the product of BC optical depth and cloud fraction as a measure of the coexistence of BC and clouds in the same atmospheric column. This weighting does not change the sign of the difference in characteristic heights. We see from Fig. 7 that the differences of cloudy- minus clear-sky forcings (Fig. 7-left) usually correspond to regions where BC position is below cloud (Fig. 7-right). These regions are in general land regions and mainly emission regions for BC (central Africa, Northern India, East Asia and South America). On the contrary, the regions where clouds enhance BC forcing and make it very positive (dRF > 0) are mainly over the ocean downwind from source regions (especially West Africa and East Asia). In these regions BC is mainly at an altitude higher than clouds.

5.2 Nonlinear combination of species forcing to total aerosol forcing

We discuss in this section the forcing effect of the presence, in the same atmospheric column, of layers of different aerosol species, neglecting the effect of clouds. In general,

ACPD
13, 18809–18853, 2013

the total aerosols forcing RF_{CS}(AER) differs from the sum of the forcings from individual species, as already pointed out in other studies (e.g. Boucher et al., 2001; Reddy et al., 2005). We analyse the behaviour of the total clear-sky aerosol forcing and the forcings per-species, in connection with the aerosol vertical distribution, for the "default configuration" and "aib" experiment. Consider the difference between the forcing of all aerosol components "AER" and the sum of the individual forcings:

$$\begin{aligned} dRF &= RF_{CS}(AER) - \sum RF_{CS}(spec) \\ &= RF_{CS}(AER) - RF_{CS}(BC) - RF_{CS}(SO_4) - RF_{CS}(POM) - RF_{CS}(DUST) - RF_{CS}(SS) \end{aligned}$$

The horizontal distribution of this difference, or nonlinearity, is shown in Fig. 8 (left). On global average, dRF amounts to about 14 % on global average (see Table 1, "AER" and "SUM" columns for RF_{CS}), but it can reach values of 100 % regionally (compare Fig. 8, left, to Fig. 2, top left). The difference is due to the superposition of several aerosol layers, and not due to an internally mixed aerosol, as the approach taken in these simulations is to treat the aerosol as an external mixture. However, note that the computation of RF of each species is done independently of that of the others by double calls to the radiation code. The total aerosol "AER" RF is computed by first computing a volume weighted single scattering albedo and asymmetry factor. In analogy to Fig. 7, Fig. 8 shows the horizontal distribution of the nonlinearity term dRF aside the difference of the characteristic height of BC optical depth and that of the AOD sum of the other species ("SCAT" = "SO_4" + "POM" + "DUST" + "SS"). The latter are assembled as they all have a prevailing scattering behaviour and negative forcings. The monthly height differences are multiplied by the product of the vertically integrated AOD_{BC} and AOD_{SCAT} to give more importance to the regions where significant amounts of BC and the other species are found in the same atmospheric columns. Similar to the analysis in Sect. 5.1, the regions with negative (positive) dRF usually correspond to regions where BC is lower (higher) in the atmosphere than the scattering aerosols associated with other species.

ACPD
13, 18809–18853, 2013

6 Conclusions

This study allowed to evaluate the importance of the vertical distribution of aerosols and clouds in the estimation of aerosol radiative forcing with a general circulation model. We have developed a method to study and quantify the contribution of different parts of the atmospheric column to the aerosol radiative forcing in the presence of clouds. We contrast the contribution from the different components of the aerosols from below, from inside and from above clouds to that forcing. Two different three-dimensional fields of aerosols and clouds, coming from respectively the LMDz and the SPRINTARS model, were used to investigate the potential impact of vertical distribution on inter-model forcing differences. We used a general circulation model with a radiation module for the aerosols to study at the same time the physical mechanisms of interaction of light with several superposed layers, and their importance on the global scale.

This study illustrates the importance of the nonlinearity that arises from the vertical superposition of different atmospheric components, by quantifying the difference between the total forcing and the sum of the forcings, and the dependency of a single-component forcing on the presence and vertical distribution of the others. We investigated this phenomenon both for the superposition of aerosols (primarily BC) and clouds, and of different aerosol species together or computed separately. We have shown that nonlinear effects when superposing several aerosol species are not negligible, especially when considered regionally: the total aerosol forcing, computed assuming that the individual forcings sum up linearly, can differ from the actual value up to 100 %, and the difference amounts to 14 % on global average. A simple approximation to zero-order in the transmittances of the atmospheric components allows to predict the sign of this nonlinearity according to which species is lower in the atmospheric column. The non-linearity is partly explained by the respective position of BC and the scattering part of the aerosol. In turn this means that BC forcing should not be computed alone. BC forcing might be considerably overestimated in case of scattering aerosols being overestimated below the BC rich layers.

ACPD
13, 18809–18853, 2013

These nonlinear effects are even more important when superposing aerosols (in particular absorbing aerosols) and clouds. For example, the BC cloudy-sky forcing differs from its clear-sky counterpart by +52 % on global average. The experiments performed by splitting the realistic aerosol distribution in three parts (above, within, below clouds) allowed to attribute this increment to the different regions of the atmospheric column, quantifying at the same time the global-scale effect. In this way, the differences between cloudy- and clear-sky BC forcings amount to +163 %, +64 % and −47 % of their clear-sky counterparts, when BC is found above, within and below clouds respectively. These results reflect a strong enhancement of the forcing for BC above clouds, attenuation for BC below clouds, and a moderate enhancement when BC is found within clouds. Accordingly, BC forcing efficiency amounts to 44, 171, 333 and 178 $W m^{-2}$ per unit optical depth for BC below, within and above clouds and for the 3-D BC distribution, respectively. The overall contribution from BC within clouds (as defined in our model set-up) is as important as that of BC above clouds.

Differences between aerosol forcings from different models can have several causes (e.g. different radiation computations, surface albedo, meteorology etc.). In particular, the different behaviour of forcing nonlinearities for the regions above, within and below clouds, documented by our experiments, suggests that an important reason for differences between cloudy-sky aerosol forcings may come, ultimately, from different treatments of wet scavenging. Here we propose a method to investigate model differences and to isolate the effect of aerosols and clouds radiative interactions only, by running one model in five different configurations. First, we run our model LMDz in the "default" configuration. Then, we read into our model the aerosols and clouds fields in output from LMDz itself and from the model SPRINTARS, and we compare results. The differences can be attributed to clouds and aerosols fields of the two models because the "host model" is the same and we ruled out any feedback of read aerosols and clouds fields on meteorology. The differences between on global average are quite small, but can exceed 100 % of the "LMDz values" regionally. These differences for cloudy skies show a regional pattern that can be interpreted with the aid of the split

ACPD
13, 18809–18853, 2013

of the full BC distribution in three components. Indeed, in the regions where SPRINTARS exceeds the LMDz cloudy-sky forcing, also BC optical depth above and inside clouds are higher in SPRINTARS. To validate our results, we perform two "crossed experiments", by reading aerosols from one model and clouds from the other one. The method of splitting aerosol distribution in the three components "above", "inside" and "below" clouds helps to interpret the differences among the runs. The larger cloudy-sky forcing efficiencies are observed for the two configurations "reading SPRINTARS" and "reading LMDZ aerosols – SPRINTARS clouds", with values of 190 and 227 $W m^{-2}$ per unit optical depth. These configurations correspond to the maximum fraction of BC above and within clouds: 85 % and 88 % respectively, against 66 % and 69 % for the two other configurations. Our analysis shows that the different amount of black carbon above and within clouds in the two models is the main reason of difference in the cloudy-sky forcing efficiency, while, in the range of clouds parameters considered here, the different cloud characteristics play a minor role. Myhre et al. (2013) have reported large differences between the two models, i.e. an all-sky forcing efficiency per unit optical depth of BC from fossil and bio fuel of 122 $W m^{-2}$ (LMDZ-INCA) and 171 $W m^{-2}$ (SPRINTARS). Here we find corresponding values for all-sky forcing efficiency of total black carbon of rounded 151 $W m^{-2}$ for both LMDZ and SPRINTARS configurations, using the same host model. Although the BC fields used here are not exactly comparable to the ones used in Myhre et al. (2013), it is very likely that the larger differences in all-sky forcing efficiency in the original models are also caused by host model characteristics and not only by differences in vertical superposition of aerosol and clouds.

Appendix

Derivation of sign of total forcing minus the sum of individual forcings

Consider two generic absorbing/scattering short-lived atmospheric components (they can be two different aerosol layers or an aerosol and a cloud layer) "B" and "C"; we

ACPD
13, 18809–18853, 2013

use "A" to refer to the clear-sky atmosphere. We are interested in the difference between the forcing when B and C are superposed and when they are juxtaposed. In a plane parallel atmosphere approximation, the forcings can be expressed in terms of the bulk transmittance, reflectance and absorbance of the components (Chylek et al., 1997). The upward TOA flux coming from the agent B alone, to the lowest order in the transmittances, can be written as:

$$F_{+}^{\mathrm{B}} = R_{\mathrm{A}}F + T_{\mathrm{A}}T_{\mathrm{A}}'' R_{\mathrm{B}}F, \tag{A1}$$

where F is the incoming solar flux, R_{A} and R_{B} indicate the atmosphere and the component B reflectances, respectively, and T_{A} and T_{A}'' are the transmittances of the atmosphere above B for the incoming and outgoing radiation respectively (the transmittances depend on the spectral distribution of the radiation). Figure 1 (center) describes this situation. In Eq. (A1) we neglected the terms of order aT_{B}^2 (a is the surface albedo) and higher-order terms; as $a < 1$, $T_{\mathrm{B}} < 1$, we expect these higher-order terms to be less important than the ones in Eq. (A1); nevertheless, this approximation will be quite rough for optically thin atmospheric agents (large T_{B}) and high surface albedo. Analogously, the outgoing flux in clear-sky conditions can be written as:

$$F_{+}^{\mathrm{A}} = R_{\mathrm{A}}F + t_{\mathrm{A}}t_{\mathrm{A}}'' a\, F, \tag{A2}$$

(see Fig. 1, left) where a is the surface albedo, t and t'' are the transmittances in clear-sky conditions. Equation (A1) can be approximated assuming that the two way-atmospheric transmittance is a constant (Corti et al., 2009): $T_{\mathrm{A}}T_{\mathrm{A}}'' = t_{\mathrm{A}}t_{\mathrm{A}}'' = k_{\mathrm{A}}$. This allows approximating the expression for the forcing by the atmospheric agent B in the following way:

$$\mathrm{RF}^{\mathrm{B}} = \left(F - F_{+}^{\mathrm{B}}\right) - \left(F - F_{+}^{\mathrm{A}}\right) \approx k_{\mathrm{A}}F(a - R_{\mathrm{B}}). \tag{A3}$$

This expression implies that the forcing is proportional to the change in reflectivity with respect to the surface albedo, due to the presence of B.

ACPD
13, 18809–18853, 2013

In the case the B layer is found above C (see Fig. 1, right), and still neglecting second order terms in the transmittances of B and C, we can approximate the net flux with the expression (Eq. A1) and the total forcing with the expression (Eq. A3), that is:

$$F_{+,s}^{B+C} \approx R_A F + T_A T_A'' R_B F$$
$$RF_s^{B+C} \approx RF^B, \quad \text{(A4)}$$

where the subscript "s" denotes that B and C are superposed. As shown in Fig. 1 (right), in this way we neglect the terms of order $R_C T_B^2$ (R_C is the reflectance of the underlying component C) and higher-order terms (analogously with the approximation of Eq. (A1) with respect to terms of order aT_B^2 and higher). Then, this approximation will be rough for optically thin atmospheric components superposed to high-reflectance ones.

If the two atmospheric agents B and C are horizontally juxtaposed rather than vertically superposed, the total forcing will be simply the sum of the forcings:

$$RF_0^{B+C} \approx RF^B + RF^C \quad \text{(A5)}$$

In this way, the difference between the forcing in the "juxtaposed" and "superposed" situation is:

$$RF_0^{B+C} - RF_s^{B+C} \approx -RF^C \quad \text{(A6)}$$

that is, the main contribution to the nonlinearity is the opposite of the forcing of the underlying species (C in this case). As Eq. (A4), this approximation will be quite rough if B is optically thin and C highly reflective. But we are interested here only to the dominant behaviour and we investigate how much the approximation (Eq. A6) is useful to interpret the results of a GCM.

If the species B and C are aerosols and clouds without dynamical/microphysical interactions, the difference (A6) corresponds to the difference between cloudy-sky and clear-sky forcings, as explained in Sect. 2. Thus, if clouds are below the aerosol B, the

ACPD
13, 18809–18853, 2013

approximation (Eq. A6) implies that the difference between the cloudy and the clear-sky forcing will be usually positive, as it is dominated by the opposite of the forcing from clouds (that is mainly negative).

Acknowledgements. This work was granted access to the HPC resources of [CCRT/TGCC/CINES/IDRIS] under the allocation 2012-t2012012201 made by GENCI (Grand Equipement National de Calcul Intensif). We also thank Brigitte Koffi for the fruitful discussions about clouds and aerosol vertical profiles. This study has been supported under European Commission framework contracts EUCAARI (no. 036833-2) and ECLIPSE (no. 282688).

The publication of this article is financed by CNRS-INSU.

References

Albrecht, B. A.: Aerosols, cloud microphysics, and fractional cloudiness, Science, 245, 1227–1230, 1989.

Bellouin, N., Jones, A., Haywood, J., and Christopher, S. A.: Updated estimate of aerosol direct radiative forcing from satellite observations and comparison against the Hadley Centre climate model, J. Geophys. Res., 113, D10205, doi:10.1029/2007JD009385, 2008.

Boucher, O. and Haywood, J.: On summing the components of radiative forcing of climate change, Clim. Dynam., 18, 297–302, 2001.

Boucher, O. and Pham, M.: History of sulfate aerosol radiative forcings, Geophys. Res. Lett., 29, 1308, doi:10.1029/2001GL014048, 2002.

Chand, D., Anderson, T. L., Wood, R., Charlson, R. J., Hu, Y., Liu, Z., and Vaughan, M.: Quantifying above-cloud aerosol using spaceborne lidar for improved understanding of cloudy-sky direct climate forcing, J. Geophys. Res., 113, D13206, doi:10.1029/2007JD009433, 2008.

ACPD

13, 18809–18853, 2013

Chand, D., Wood, R., Anderson, T. L., Satheesh, S. K., and Charlson, R. J.: Satellite-derived direct radiative effect of aerosols dependent on cloud cover, Nat. Geosci., 2, 181–184, doi:10.1038/NGEO437, 2009.

Charlson, R. J., Schwartz, S. E., Hales, J. M., Cess, R. D., Coakley, J. A., Hansen, J. E., and Hofmann, D. J.: Climate forcing by anthropogenic aerosols, Science, 255, 423–430, 1992.

Chepfer, H., Bony, S., Winker, D., Chiriaco, M., Dufresne, J., and Sèze, G.: Use of CALIPSO lidar observations to evaluate the cloudiness simulated by a climate model, Geophys. Res. Lett., 35, L15804, doi:10.1029/2008GL034207, 2008.

Chylek, P. and Wong, J. G. D.: Cloud radiative forcing ratio – an analytical model, Tellus A, 50, 259–264, 1998.

Conant, W. C., Seinfeld, J. H., Wang, J., Carmichael, G. R., Tang, Y., Uno, I., Flatau, P. J., Markowicz, K. M., and Quinn, P. K.: A model for the radiative forcing during ACE-Asia derived from CIRPAS Twin Otter and R/V *Ronal H. Brown* data and comparison with observations, J. Geophys. Res., 108, D23, 8661, doi:10.1029/2002JD003260, 2003.

Cooke, W. F. and Wilson, J. J. N.: A global black carbon aerosol model, J. Geophys. Res., 101, 19395–19409, 1996.

Corti, T. and Peter, T.: A simple model for cloud radiative forcing, Atmos. Chem. Phys., 9, 5751–5758, doi:10.5194/acp-9-5751-2009, 2009.

Evan, A. T., Vimont, D. J., Heidinger, A. K., Kossin, J. P., and Bennartz, R.: The role of aerosols in the evolution of tropical North Atlantic Ocean temperature anomalies, Science, 324, 778–781, doi:10.1126/science.1167404, 2009.

Fouquart, Y. and Bonnel, B.: Computations of solar heating of the Earth s atmosphere: a new parameterization, Beitr. Phys. Atmos., 53, 35–62, 1980.

Gerber, H. E.: Atmospheric aerosols and nucleation, in: Lecture Notes Physics, edited by: W. Beiglbock, New York, USA, 237–238, 1988.

Gomez-Amo, J. L., di Sarra, A., Meloni, D., Cacciani, M., and Utrillas, M. P.: Sensitivity of shortwave radiative fluxes to the vertical distribution of aerosol single scattering albedo in the presence of a desert dust layer, Atmos. Environ., 44, 2787–2791, doi:10.1016/j.atmosenv.2010.04.041, 2010.

Hansen, J., Sato, M., and Ruedy, R.: Radiative forcing and climate response, J. Geophys. Res., 102, 6831–6864, doi:10.1029/96JD03436, 1997.

ACPD
13, 18809–18853, 2013

Haywood, J. M. and Ramaswamy, V.: Global sensitivity studies of the direct radiative forcing due to anthropogenic sulfate and black carbon aerosols, J. Geophys. Res., 103, 6043–6058, 1998.

Haywood, J. M. and Shine, K. P.: Multi-spectral calculations of the direct radiative forcing of tropospheric sulphate and soot aerosols using a column model, Q. J. Roy. Meteor. Soc., 123, 1907–1930, 1997.

Hourdin, F., Musat, I., Bony, S., Braconnot, P., Codron, F., Dufresne, J.-L., Fairhead, L., Filiberti, M.-A., Friedlingstein, P., Grandpeix, J.-Y., Krinner, G., Levan, P., Li, Z.-X., and Lott, F.: The LMDZ4 general circulation model: climate performance and sensitivity to parametrized physics with emphasis on tropical convection, Clim. Dynam., 27, 787–813, 2006.

Koffi, B., Schulz, M., Breon, F.-M., Griesfeller, J., Winker, D., Balkanski, Y., Bauer, S., Berntsen, T., Chin, M., Collins, W. D., Dentener, F., Diehl, T., Easter, R., Ghan, S., Ginoux, P., Gong, S., Horowitz, L. W., Iversen, T., Kirkevag, A., Koch, D., Krol, M., Myhre, G., Stier, P., and Takemura, T.: Application of the CALIOP layer product to evaluate the vertical distribution of aerosols estimated by global models: AeroCom phase I results, J. Geophys. Res., 117, D10201, doi:10.1029/2011JD016858, 2012.

Li, J., Hu, Y., Huang, J., Stamnes, K., Yi, Y., and Stamnes, S.: A new method for retrieval of the extinction coefficient of water clouds by using the tail of the CALIOP signal, Atmos. Chem. Phys., 11, 2903–2916, doi:10.5194/acp-11-2903-2011, 2011.

Liao, H. and Seinfeild, J. H.: Radiative forcing by mineral dust aerosols: sensitivity to key variables, J. Geophys. Res., 103, 31637–31645, 1998.

Meloni, D., Sarra, A. D., Iotio, T. D., and Fiocco, G.: Influence of the vertical profile of Saharan dust on the visible direct radiative forcing, J. Quant. Spectrosc. Ra., 93, 497–413, 2005.

Morcrette, J. J. and Fouquart, Y.: The overlapping of cloud layers in shortwave radiation parameterizations, J. Atmos. Sci., 43, 321–328, 1986.

Myhre, G., Samset, B. H., Schulz, M., Balkanski, Y., Bauer, S., Berntsen, T. K., Bian, H., Bellouin, N., Chin, M., Diehl, T., Easter, R. C., Feichter, J., Ghan, S. J., Hauglustaine, D., Iversen, T., Kinne, S., Kirkevåg, A., Lamarque, J.-F., Lin, G., Liu, X., Lund, M. T., Luo, G., Ma, X., van Noije, T., Penner, J. E., Rasch, P. J., Ruiz, A., Seland, Ø., Skeie, R. B., Stier, P., Takemura, T., Tsigaridis, K., Wang, P., Wang, Z., Xu, L., Yu, H., Yu, F., Yoon, J.-H., Zhang, K., Zhang, H., and Zhou, C.: Radiative forcing of the direct aerosol effect from AeroCom Phase II simulations, Atmos. Chem. Phys., 13, 1853–1877, doi:10.5194/acp-13-1853-2013, 2013.

ACPD
13, 18809–18853, 2013

Peters, K., Quaas, J., and Bellouin, N.: Effects of absorbing aerosols in cloudy skies: a satellite study over the Atlantic Ocean, Atmos. Chem. Phys., 11, 1393–1404, doi:10.5194/acp-11-1393-2011, 2011.

Podgorny, I. A. and Ramanathan, V.: A modeling study of the direct effect of aerosols over the tropical Indian Ocean, J. Geophys. Res., 106, 24097–24105, 2001.

Quaas, J., Boucher, O., and Breon, F. M.: Aerosol indirect effects in POLDER satellite data and the Laboratoire de Meteorologie Dynamique-Zoom (LMDZ) general circulation model, J. Geophys. Res., 109, D08205, doi:10.1029/2003JD004317, 2004.

Rayner, N. A., Parker, D. E., Horton, E. B., Folland, C. K., Alexander, L. V., Rowell, D. P., Kent, E. C., and Kaplan, A.: Global analyses of sea surface temperature, sea ice, and night marine air temperature since the late nineteenth century, J. Geophys. Res., 108, 4407, doi:10.1029/2002JD002670, 2003.

Reddy, M. S., Boucher, O., Balkanski, Y., and Schulz, M.: Aerosol optical depths and direct radiative perturbations by species and source type, Geophys. Res. Lett., 32, L12803, doi:10.1029/2004GL021743, 2005.

Samset, B. H. and Myhre, G.: Vertical dependence of black carbon, sulphate and biomass burning aerosol radiative forcing, Geophys. Res. Lett., 38, L24802 doi:10.1029/2011gl049697, 2011.

Samset, B. H., Myhre, G., Schulz, M., Balkanski, Y., Bauer, S., Berntsen, T. K., Bian, H., Bellouin, N., Diehl, T., Easter, R. C., Ghan, S. J., Iversen, T., Kinne, S., Kirkevåg, A., Lamarque, J.-F., Lin, G., Liu, X., Penner, J. E., Seland, Ø., Skeie, R. B., Stier, P., Takemura, T., Tsigaridis, K., and Zhang, K.: Black carbon vertical profiles strongly affect its radiative forcing uncertainty, Atmos. Chem. Phys., 13, 2423–2434, doi:10.5194/acp-13-2423-2013, 2013.

Satheesh, S. K., Ramanathan, V., Jones, X., Lobert, J. M., Podgorny, I. H., Prospero, J. M., Holben, B. N., and Loeb, N. G.: A model for the natural and anthropogenic aerosols over the tropical Indian Ocean derived from Indian Ocean Experiment data, J. Geophys. Res., 104, 27421–27440, 1999.

Schulz, M., Textor, C., Kinne, S., Balkanski, Y., Bauer, S., Berntsen, T., Berglen, T., Boucher, O., Dentener, F., Guibert, S., Isaksen, I. S. A., Iversen, T., Koch, D., Kirkevåg, A., Liu, X., Montanaro, V., Myhre, G., Penner, J. E., Pitari, G., Reddy, S., Seland, Ø., Stier, P., and Takemura, T.: Radiative forcing by aerosols as derived from the AeroCom present-day and pre-industrial simulations, Atmos. Chem. Phys., 6, 5225–5246, doi:10.5194/acp-6-5225-2006, 2006.

ACPD
13, 18809–18853, 2013

Simmons, A., Uppala, S., Dee, D., and Kobayashi, S.: ERA-Interim: new ECMWF reanalysis products from 1989 onwards, ECMWF Newsletter articles, 110, 25–35, 2006.
Takemura, T., Nakajima, T., Dubovik, O., Holben, B. N., and Kinne, S.: Single scattering albedo and radiative forcing of various aerosol species with a global three-dimensional model, J. Climate, 15, 333–352, 2002.
Takemura, T., Nozawa, T., Emori, S., Nakajima, T., and Nakajima, T.: Simulation of climate response to aerosol direct and indirect effects with aerosol transport-radiation model, J. Geophys. Res., 110, D02202, doi:10.1029/2004JD005029, 2005.
Turpin, B. J. and Lim, H. J.: Species contributions to $PM_{2.5}$ mass concentrations: revisiting common assumptions for estimating organic mass, Aerosol Sci. Tech., 35, 602–610, 2001.
Twomey, S.: Pollution and the planetary albedo, Atmos. Environ., 8, 1251–1256, 1974.
Twomey, S.: Aerosols, clouds, and radiation, Atmos. Environ., 25, 2435–2442, 1991.
Visser, H., Folkert, R. J. M., Hoekstra, J., and de Wolff, J. J.: Identifying key sources of uncertainty in climate change projections, Climatic Change, 45, 421–457, 2000.
Vuolo, M. R., Chepfer, H., Menut, L., and Cesana, G.: Comparison of mineral dust layers vertical structures modelled with Chimere-Dust and observed with the Caliop lidar, J. Geophys. Res., 114, 1984–2012, doi:10.1029/2008JD011219, 2009.
Zarzycki, C. M. and Bond, T. C.: How much can the vertical distribution of black carbon affect its global direct radiative forcing?, Geophys. Res. Lett., 37, L20807, doi:10.1029/2010gl044555, 2010.

ACPD
13, 18809–18853, 2013

Table 1. Characteristic properties of the "reference simulation" using the "default configuration" of LMDz with the full aerosol distribution, (above, inside, below clouds, including the area with completely clear columns). "BC" = Black Carbon; "SO_4" = Sulphate; "POM" = Particulate Organic Matter; "DUST" = Mineral Dust; "SS" = Sea Salt; "AER" = forcing diagnostics established using instantaneous, total aerosol optical properties; "SUM" = arithmetic sum of values from individual aerosol species diagnostics. AOD = all-sky aerosol optical depth at 550 nm wavelength. AOD^* = average optical depth when excluding completely clear columns. $CLT^\#$ = Effective Cloud fraction, see text; RF = direct radiative forcing against an aerosol-free atmosphere; NRF = RF normalized to AOD; "CS" = clear-sky; "CL" = cloudy-sky only; "AS" = all-sky. Cloud mask hypothesis derived all-sky forcings $RF^*_{AS} = (1 - CLT) \cdot RF_{CS}$.

	BC	SO_4	POM	DUST	SS	AER	SUM
AOD [1]	2.71×10^{-3}	3.96×10^{-2}	1.77×10^{-2}	2.67×10^{-2}	3.89×10^{-2}	0.126	0.126
AOD^* [1]	2.37×10^{-3}	3.59×10^{-2}	1.61×10^{-2}	1.84×10^{-2}	3.74×10^{-2}	0.110	0.110
Burden [$\mu g\,m^{-2}$]	0.288	3.23	2.30	34.6	38.1	78.5	78.5
$CLT^\#$ [%]	39 %	44 %	41 %	30 %	58 %	47 %	39 %
Forcings							
RF_{CS}[$W\,m^{-2}$]	0.280	−0.730	−0.253	−0.473	−0.913	−2.39	−2.09
RF_{CL} [$W\,m^{-2}$]	0.425	−0.190	0.031	−0.130	−0.121	−0.101	0.0146
RF_{AS} [$W\,m^{-2}$]	0.378	−0.466	−0.119	−0.342	−0.428	−1.19	−0.979
$RF_{AS}{}^*$ [$W\,m^{-2}$]	0.17	−0.41	−0.15	−0.33	−0.38	−1.27	
Forcing efficiencies							
NRF_{CS}[$W\,m^{-2}/1$]	104	−18.4	−14.3	−17.7	−23.5	−19.0	–
NRF_{CL}[$W\,m^{-2}/1$]	157	−4.79	1.75	−4.89	−3.11	−0.801	–

ACPD
13, 18809–18853, 2013

Table 2. Optical depth and forcings in four experiments with aerosols above + inside + below clouds ("aib"), only above ("abv"), only inside ("in") and only below clouds ("blw") using the "default configuration"; averages exclude completely clear columns. Abbreviations as in Table 1.

	BC	SO_4	POM	DUST	SS	AER	SUM
			AIB Experiment				
AOD*1000 [1]	2.4	35.9	16.1	18.4	37.4	110	110
RF_{CS} [Wm^{-2}]	+0.279	−0.725	−0.252	−0.464	−0.910	−2.370	−2.070
RF_{CL} [Wm^{-2}]	+0.424	−0.189	+0.031	−0.130	−0.121	−0.100	+0.015
$(RF_{CL} - RF_{CS})/\lvert RF_{CS}\rvert$	**52 %**	**74 %**	**112 %**	**72 %**	**87 %**	**96 %**	
RF_{AS} [Wm^{-2}]	+0.375	−0.463	−0.119	−0.334	−0.427	−1.180	−0.968
NRF_{CS} [$Wm^{-2}/1$]	+118	−20,2	−15.6	−25.2	−24.4	−21.5	–
NRF_{CL} [$Wm^{-2}/1$]	+178	−5.3	+1.9	−7.0	−3.2	−0.9	–
			ABV Experiment				
AOD*1000 [1]	0.69	10.6	4.83	2.17	2.51	20.8	20.8
RF_{CS} [Wm^{-2}]	+0.088	−0.227	−0.064	−0.054	−0.033	−0.349	−0.289
RF_{CL} [Wm^{-2}]	+0.231	−0.057	+0.059	+0.025	+0.014	+0.257	+0.272
$(RF_{CL} - RF_{CS})/\lvert RF_{CS}\rvert$	**163 %**	**75 %**	**192 %**	**146 %**	**142 %**	**174 %**	
RF_{AS}[Wm^{-2}]	+0.163	−0.130	+0.001	−0.012	−0.008	−0.022	−0.008
NRF_{CS}[$Wm^{-2}/1$]	+126	−21.3	−13.2	−24.8	−13.2	−16.7	–
NRF_{CL}[$Wm^{-2}/1$]	+333	−5.4	+12.2	+11.5	+5.7	+12.3	–
			IN Experiment				
AOD*1000 [1]	0.85	16.4	6.50	4.68	19.2	47.6	47.6
RF_{CS}[Wm^{-2}]	+0.089	−0.264	−0.084	−0.126	−0.446	−0.993	−0.831
RF_{CL}[Wm^{-2}]	+0.146	−0.048	+0.018	−0.002	−0.042	+0.019	+0.071
$(RF_{CL} - RF_{CS})/\lvert RF_{CS}\rvert$	**64 %**	**82 %**	**121 %**	**98 %**	**91 %**	**102 %**	
RF_{AS}[Wm^{-2}]	+0.120	−0.131	−0.030	−0.057	−0.156	−0.358	−0.254
NRF_{CS}[$Wm^{-2}/1$]	+104	−16.1	−12.9	−26.8	−23.3	−20.9	–
NRF_{CL}[$Wm^{-2}/1$]	+171	−2.9	2.7	−0.52	−2.2	+0.4	–
			BLW Experiment				
AOD*1000 [1]	0.83	8.91	4.78	11.5	15.7	41.8	41.8
RF_{CS}[Wm^{-2}]	+0.068	−0.171	−0.085	−0.193	−0.418	−0.895	−0.800
RF_{CL}[Wm^{-2}]	+0.036	−0.072	−0.041	−0.138	−0.089	−0.353	−0.303
$(RF_{CL} - RF_{CS})/\lvert RF_{CS}\rvert$	**−47 %**	**58 %**	**52 %**	**28 %**	**79 %**	**61 %**	
RF_{AS}[Wm^{-2}]	+0.057	−0.136	−0.070	−0.171	−0.242	−0.637	−0.561
NRF_{CS}[$Wm^{-2}/1$]	+82	−19.2	−17.8	−16.7	−26.7	−21.4	–
NRF_{CL}[$Wm^{-2}/1$]	+44	−8.1	−8.6	−11.9	−5.7	−8.5	–

ACPD
13, 18809–18853, 2013

Table 3. Black carbon optical depth (AOD_{BC}) and associated forcings for 4 experiments (as detailed in Table 2) and 4 configurations in which monthly LMDzT and SPRINTARS aerosol and cloud fields are read. Abbreviations as in Table 1.

Experiments:	AIB	ABV	IN	BLW
Reading LMDZ aerosol and cloud configuration (corresponding to Table 2 reference simulation)				
AOD_{BC}*1000 [1]	2.47	0.72	0.99	0.75
RF_{CS} [Wm^{-2}]	0.279	0.092	0.096	0.065
RF_{AS} [Wm^{-2}]	0.372	0.164	0.124	5.71×10^{-2}
RF_{CL} [Wm^{-2}]	0.442	0.237	0.153	3.79×10^{-2}
NRF_{CS} [Wm^{-2}/1]	113	127	96.6	86.5
NRF_{CL} [Wm^{-2}/1]	179	328	155	50
Reading SPRINTARS aerosol and cloud configuration				
AOD_{BC}*1000 [1]	2.32	0.75	1.24	0.33
RF_{CS} [Wm^{-2}]	0.270	0.084	0.106	0.028
RF_{AS} [Wm^{-2}]	0.351	0.147	0.127	0.025
RF_{CL} [Wm^{-2}]	0.440	0.237	0.157	0.015
NRF_{CS} [Wm^{-2}/1]	116	112	85.3	86.1
NRF_{CL} [Wm^{-2}/1]	190	318	127	44
Reading LMDZ aerosols – reading SPRINTARS clouds configuration				
AOD_{BC}*1000 [1]	2.21	0.99	0.95	0.27
RF_{CS} [Wm^{-2}]	0.278	0.117	0.083	0.023
RF_{AS} [Wm^{-2}]	0.383	0.208	0.101	0.020
RF_{CL} [Wm^{-2}]	0.500	0.329	0.126	0.012
NRF_{CS} [Wm^{-2}/1]	126	118	87	84.1
NRF_{CL} [Wm^{-2}/1]	227	333	132	43.6
Reading SPRINTARS aerosols – reading LMDZ clouds configuration				
AOD_{BC}*1000 [1]	2.58	0.51	1.18	0.89
RF_{CS} [Wm^{-2}]	0.271	0.062	0.107	0.078
RF_{AS} [Wm^{-2}]	0.342	0.113	0.138	0.067
RF_{CL} [Wm^{-2}]	0.383	0.164	0.163	0.043
NRF_{CS} [Wm^{-2}/1]	105	122	90.4	87.1
NRF_{CL} [Wm^{-2}/1]	148	321	138	48.7

ACPD
13, 18809–18853, 2013

Table 4. Clouds characteristics for the "default", "Reading LMDZ" and "Reading SPRINTARS" configurations: cloud optical depth (COD) and 2-D cloud fraction (CLT).

	Default configuration	Reading LMDZ configuration	Reading SPRINTARS configuration
COD	6.76	6.76	7.91
CLT	0.463	0.435	0.396

ACPD
13, 18809–18853, 2013

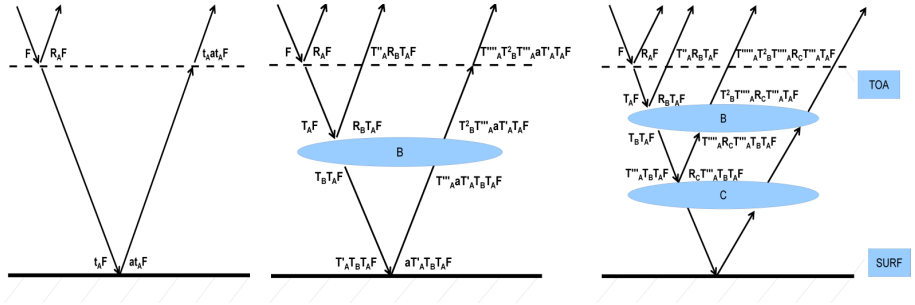

Fig. 1. Illustration of the computation of net fluxes at the top of the atmosphere (TOA) for completely clear-sky (left), in the presence of an atmospheric agent "B" (center) and in presence of two superposed atmospheric agents "B" and "C" (right). For simplicity of reading, at each interaction between the flux and an atmospheric agent, we indicate as first factor the coefficient that describes the last modification of the flux. t, T = transmissivities for clear sky and with the presence of an atmospheric agent respectively; R = reflectivity; a = surface albedo. For a given atmospheric layer, $T + R + A = 1$ (A = absorptivity). Transmissivity is related to the optical depth τ by the relation $T = \exp(-\tau)$.

ACPD
13, 18809–18853, 2013

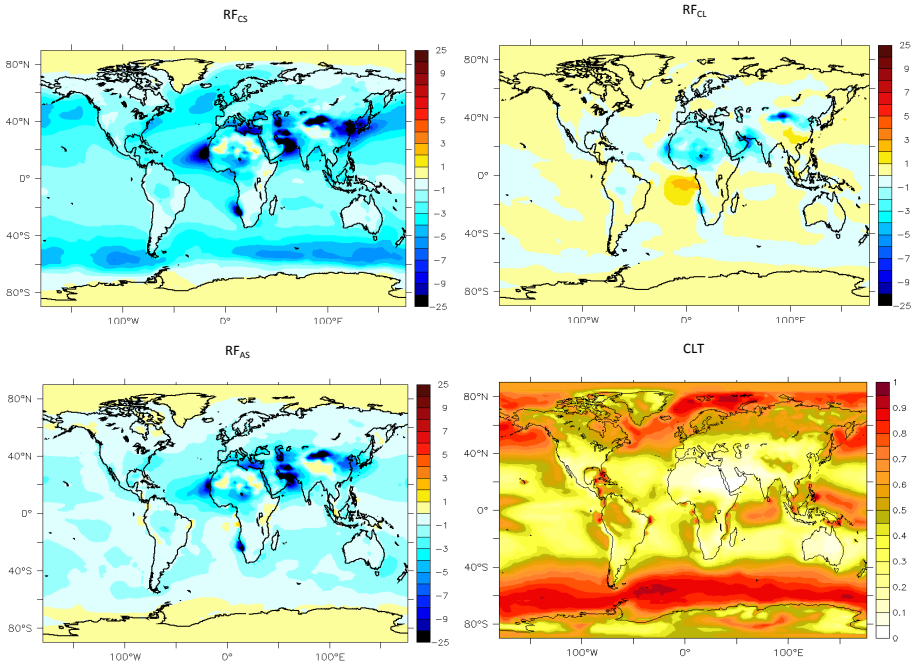

Fig. 2. All-aerosol (AER) radiative forcing in clear-sky (RF_{CS} [$W\,m^{-2}$], top left), cloudy-sky (RF_{CL} [$W\,m^{-2}$], top right) and all-sky (RF_{AS} [$W\,m^{-2}$], bottom left) conditions. Bottom right: cloud fraction (CLT[1]).

ACPD
13, 18809–18853, 2013

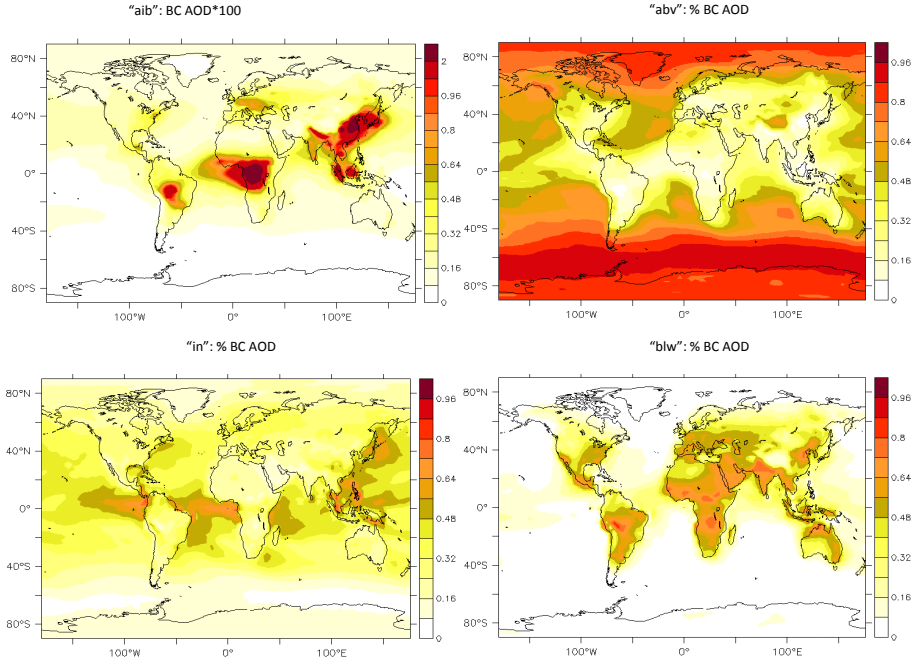

Fig. 3. BC optical depth distribution: BC AOD*100 for the "aib" experiment (top left); percentage of BC AOD above clouds ("abv" experiment, top right); percentage of BC AOD inside clouds ("in" experiment, bottom left) and percentage of BC AOD below clouds ("blw" experiment, bottom right).

ACPD
13, 18809–18853, 2013

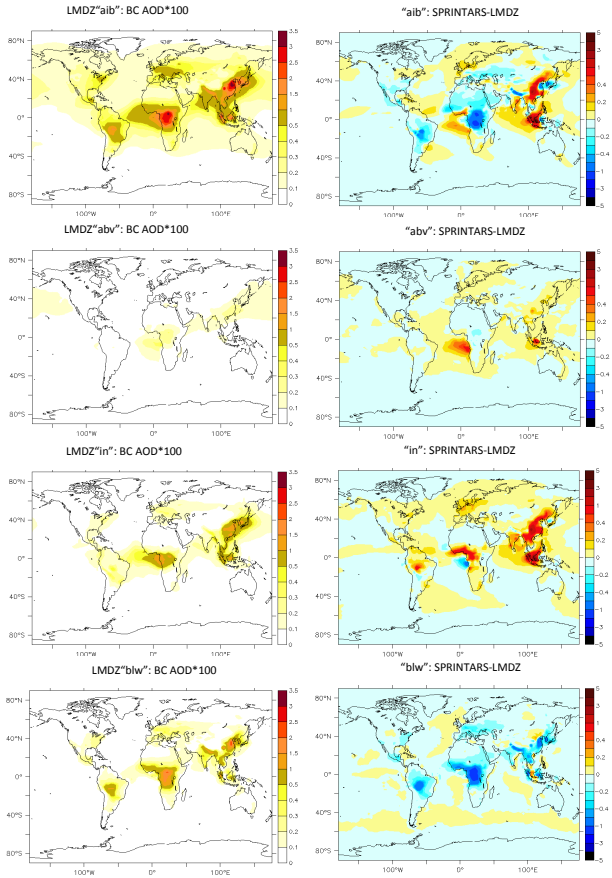

Fig. 4. Left column: "LMDZ-reading" values of BC optical depth (BC AOD). Right column: "SPRINTARS-reading" minus "LMDZ-reading" values of BC AOD. Top to bottom: "aib", "abv", "in" and "blw" experiments.

ACPD
13, 18809–18853, 2013

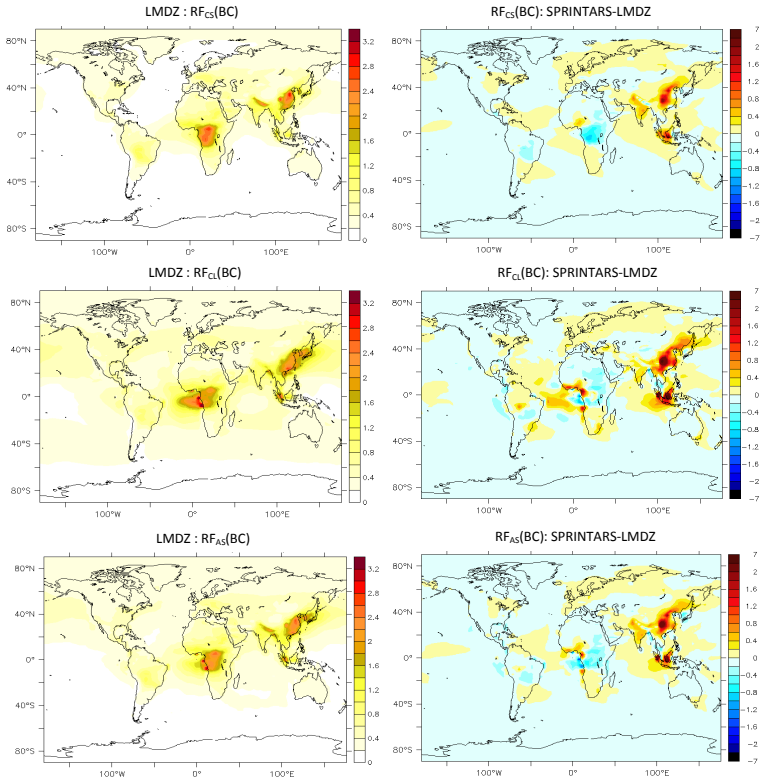

Fig. 5. Left column: "LMDZ-reading" values of BC forcings. Right column: "SPRINTARS-reading" minus "LMDZ-reading" BC forcings. Top to bottom: clear-, cloudy- and all-sky values (RF_{CS}, RF_{CL}, RF_{AS} [$W m^{-2}$]).

ACPD
13, 18809–18853, 2013

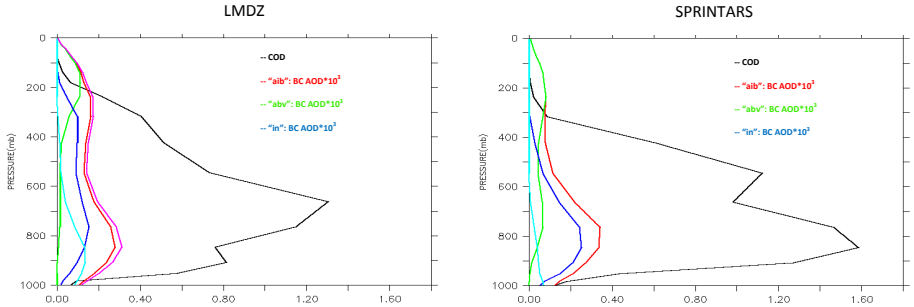

Fig. 6. Vertical profiles of BC and cloud optical depths (BC AOD and COD), for "reading LMDZ" (left) and "reading SPRINTARS" (right) configurations, and "aib", "abv", "in", "blw" experiments. In the left figure, we also plot for comparison the vertical profile of BC AOD for the default 3-D distribution experiment (aerosols also in completely clear columns).

ACPD
13, 18809–18853, 2013

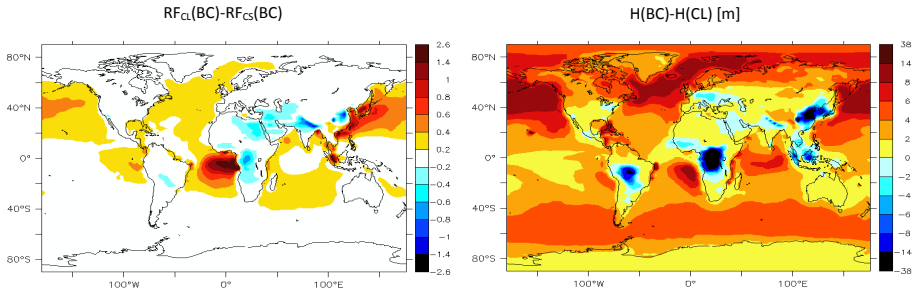

Fig. 7. Left: difference between cloudy- and clear-sky BC forcing ($RF_{CL}(BC)$ [$W\,m^{-2}$], $RF_{CS}(BC)$ [$W\,m^{-2}$]) for the "aib" experiment. Right: characteristic height (see text for definition) of BC optical depth (H(BC)[m]) minus characteristic height of clouds optical depth (H(CL) [m]). The differences in heights are multiplied by the monthly product of the 2-D BC optical depth and the 2-D cloud fraction.

ACPD
13, 18809–18853, 2013

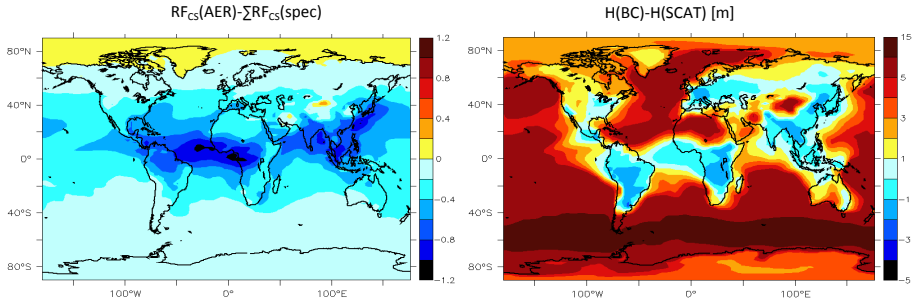

Fig. 8. Left: difference between the actual total aerosol forcing, $RF_{CS}(AER)$ [$W m^{-2}$], and the sum of forcings per species, $\sum RF_{CS}(spec)$ [$W m^{-2}$]. Right: characteristic height of BC AOD, $H(BC)$ [m], minus characteristic height of the ensemble AOD of the other species, $H(SCAT)$ [m]. The differences in heights are multiplied by the product of the 2-D optical depth of BC and of the ensemble AOD of the other species.

ACPD
13, 18809–18853, 2013